ACS APPLIED MATERIALS & INTERFACES

Research Article

www.acsami.org

Nanoparticle Flotation Collectors III: The Role of Nanoparticle Diameter

Songtao Yang, Robert Pelton,* Miles Montgomery, and Yuguo Cui

Department of Chemical Engineering, McMaster University, 1280 Main Street West, Hamilton, Ontario, Canada L8S 4L7

Supporting Information

ABSTRACT: The ability of polystyrene nanoparticles to promote glass bead flotation was measured as a function of nanoparticle diameter. In all cases, smaller nanoparticles were more effective flotation collectors, even when compared at constant nanoparticle number concentration. The superior performance of smaller particles was explained by two mechanisms, acting in parallel. First, smaller particles deposit more quickly giving more effective flotation in those cases where nanoparticle deposition kinetics is rate determining; the sensitivity of nanoparticle deposition rates to particle size was illustrated by kinetic measurements on a quartz crystal microbalance silica surface. Second, for a given coverage of nanoparticles on the glass beads, the mean distance between neighboring nanoparticle surfaces decreases with particle diameter. We propose that the expansion of the three phase contact line, after initial bead/bubble attachment, is favored with decreasing the distance between neighboring hydrophobic particles.

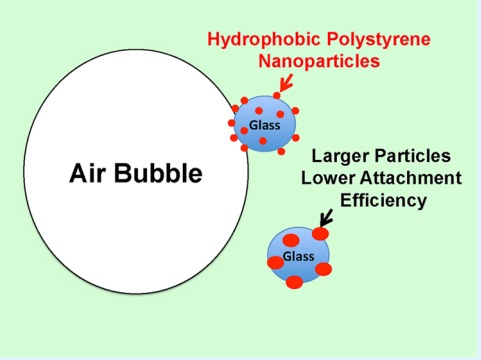

KEYWORDS: *nanoparticle deposition, flotation, deposition kinetics, contact angle, dewetting*

INTRODUCTION

We recently introduced a potential new mineral processing technology we call nanoparticle flotation collectors.[1,2] Flotation is one of the most important unit operations in mineral processing. Ores are ground to micrometer-sized particles consisting of a mixture of desired mineral-rich particles and unwanted gangue particles.[3] For many minerals, the range of particle sizes corresponding to maximum separation efficiency is in the range of 10 to 100 μm.[4] Before flotation, the ground minerals are exposed to flotation collectors to selectively render the mineral-rich particles more hydrophobic. Conventional flotation collectors are short chain surfactants with a chemi-adsorptive headgroup; amyl xanthate is a typical, conventional, molecular-sized collector. Our innovation was to replace molecular, surfactant collectors with hydrophobic nanoparticles.

In our first publication, we demonstrated that the adsorption cationic polystyrene nanoparticles onto hydrophilic glass beads facilitated bead flotation.[1] As little as 10% coverage of the bead surfaces was sufficient for flotation. Micromechanics were employed to measure directly the force required to detach individual glass beads from air bubbles. Without nanoparticles, the pull-off force was very low whereas beads with adsorbed nanoparticles gave large pull-off forces consistent with the predictions of Scheludko's model.[1,5]

The second publication in this series focused on contact angle as a predictive parameter for nanoparticle flotation performance.[2] Three types of contact angles were explored. (1) θ_{np} is the sessile drop water contact angle on smooth polymer films formed by casting polymer solutions of nanoparticles dissolved in organic solvent. This angle was taken as a measure of the hydrophobicity of the nanoparticle surfaces. By varying the surface chemistry of the nanoparticles, the minimum nanoparticle contact angle for flotation was somewhere in the range of $51° < \theta_{np} \leq 85°$. (2) θ_a is the advancing sessile drop water contact angles on dry glass surfaces decorated with nanoparticles. The receding angle could not be measured because of extreme pinning by hydrophilic patches between the nanoparticles. (3) θ_r is the captive bubble receding contact angle for submerged nanoparticle decorated glass. This measurement was the most relevant to flotation.

For every nanoparticle evaluated, $\theta_{np} > \theta_a > \theta_r$. Furthermore, the three types of contact angles gave the same flotation effectiveness ranking for our series of nanoparticles with varying surface chemistry.

The obvious nanoparticle flotation collector properties are shape, size, and surface energy. To date, we have only explored spheres with varying surface chemistry. There was an indication in the early experiments that nanoparticle size was an important parameter. Herein, we report results of a systematic investigation of particle size effects in flotation.

EXPERIMENTAL SECTION

Materials. Surfactant-free amidine white polystyrene latexes (0.76 and 2.5 μm, 4% solids) were purchased from Interfacial Dynamics Corporation (IDC, Eugene, OR). In addition, a series of nanoparticles were synthesized because the desired range of nanoparticle properties

Received: July 3, 2012
Accepted: August 7, 2012
Published: August 7, 2012

   dx.doi.org/10.1021/am301215h | ACS Appl. Mater. Interfaces 2012, 4, 4882−4890

were not commercially available; the recipes are described in the Supporting Information, and the relevant nanoparticle properties are summarized in Table 1. The flotation frother, UNIFROTH 250C (consisting of 60−100% polypropylene glycol methyl ether and 13−30% dipropylene glycol monomethyl ether), was donated by Vale Canada (Mississauga, ON). All solutions were made with Type 1 water (18.2 MΩcm, Barnstead Nanopure Diamond system). Glass beads (30−50 μm) were purchased from Polysciences, Inc. Glass beads, acid-washed (≤106 μm, −140 U.S. sieve) and unwashed (≤106 μm, −140 U.S. sieve), were purchased from Sigma-Aldrich. Particle size distributions for the beads are given in the Supporting Information.

Table 1. Some Properties of Employed Polystyrene Based Nanoparticles (Including the Purchased Ones)[a]

nanoparticle designation	hydrodynamic diameter, nm (polydispersity)	electrophoretic mobility $m^2s^{-1}V^{-1}$ (std. error)	water contact angle
NP353	353 (0.097)	$3.42 \pm 0.27 \times 10^{-8}$	88 ± 1.5
NP262	262 (0.176)	$4.27 \pm 0.21 \times 10^{-8}$	87 ± 1.8
NP292	292 (0.070)	$3.77 \pm 0.16 \times 10^{-8}$	
NP280	280 (0.108)	$-5.91 \pm 0.18 \times 10^{-8}$	92 ± 2.3
NP120	120 (0.027)	$2.74 \pm 0.12 \times 10^{-8}$	86 ± 1.1
NP79	79 (0.085)	$1.85 \pm 0.15 \times 10^{-8}$	75 ± 2.7
NP81	81 (0.149)	$2.34 \pm 0.17 \times 10^{-8}$	
NP46	46 (0.156)	$1.61 \pm 0.07 \times 10^{-8}$	93 ± 2.1
NP678	678 (0.126)	$4.43 \pm 0.31 \times 10^{-8}$	76 ± 3.5
NP2227	2227 (0.205)	$2.08 \pm 0.09 \times 10^{-8}$	86 ± 1.9

[a]Dynamic light scattering and electrophoresis were performed in 5 mM NaCl at ambient pH. Sessile drop water contact angle measured on smooth polymer films cast from nanoparticles dissolved in solvent.

Flotation. In a typical flotation experiment, 2 g of glass beads and 1.0 mL of polystyrene nanoparticle (27.15 g/L for NP353) were added into 125 mL of 5 mM NaCl, to control ionic strength, in a 150 mL plastic flotation beaker, sitting on a 90 mm diameter plastic Petri dish, which in turn was sitting on a magnetic stirrer (Corning Stirrer, Model PC-610). The suspension of glass beads and polystyrene nanoparticles was mixed (conditioned) for 5 min (25 mm × 25 mm cross-shape stirring bar at ∼600 rpm) to facilitate polystyrene nanoparticle deposition onto the glass beads. Following conditioning, 0.12 mL of 1% UNIFROTH 250C (10 ppm) was added and mixed for an additional 30 s. Flotation was commenced by initiating nitrogen flow (Matheson 604 E700 Flow Controller) at a rate of 2.0 L/min through a Corning Pyrex gas dispersion tube (Fisher Scientific, 11−137E) consisting of a 30 mm coarse glass frit attached by a 90 degrees elbow. During flotation, the stirring rate was increased to ∼900 rpm to avoid bead sedimentation. The foam phase was scraped over the edge of the beaker and collected in a plastic Petri dish. After 1.0−1.5 min, the gas flow was stopped, the plastic collection dish was replaced with a clean dish, and the liquid level in the flotation beaker was topped up with UNIFROTH 250C in 5 mM NaCl at the original concentration. In most of our flotation cases, this sequence was repeated until 3−5 dishes were collected, which is in accordance to commercial incremental flotation runs. The mass of liquid and beads collected in each dish was measured; the beads were filtered with a Büchner funnel, dried, and weighed. Typically, each dish contained 50−60 mL of flotation liquor. Flotation results were expressed as the recovery, which was calculated from the mass fraction of beads collected in the dishes. The uncertainty in the flotation results, estimated from the mass balance of glass beads, was less than 10%; for example, see the error bars in Figure 2. An example of duplicated flotation runs is given in the Supporting Information (SI Figure 4); the maximum recovery varied by about 3%.

A UV−vis spectrometer (Beckman Coulter, DU800) was used to measure the concentration of nanoparticle dispersion before and after each of the flotation runs. The extent of nanoparticle deposition on the glass beads was obtained by measuring the absorbance of the supernatant nanoparticle dispersion at 500 nm before and after deposition on the glass beads. The quantity of deposited latex was calculated using a calibration curve of absorbance versus nanoparticle concentration.

Reflotation experiments of dried recovered glass beads with nanoparticle runs were performed. Nanoparticle-treated glass beads were collected from a flotation run using nanoparticles NP79. The dried beads were weighted and added to the 150 mL plastic flotation beaker with 125 mL of 5 mM NaCl. Next, 0.12 mL of 1% UNIFROTH 250C was added and conditioned for 30 s and then subjected to flotation.

Quartz Crystal Microbalance with Dissipation (QCM-D) Measurements. Deposition of NP46, NP120, and NP262 onto silica coated sensors, which we assumed possessed similar surface characteristics as to the glass beads used in flotation, was measured using a QCM-D (E4 model from Q-Sense, Sweden). The sensors used were coated with SiO_2 (QSX303, from Q-Sense). Prior to each deposition experiment, the SiO_2 sensors were cleaned by immersing in 2% sodium dodecyl sulfate for at least 5 h followed by copious rinsing with deionized water, drying with N_2, and UV-ozone treatment (15−20 min). The baselines of the QCM-D were in equilibrium with 5 mM NaCl for ∼10 min before the nanoparticle dispersions in 5 mM NaCl were injected into the QCM-D module at 25 °C with a flow speed of 100 μL/min.

The nanoparticle coverage on the QCM-D sensor surfaces were measured directly by SEM plus image analysis. The Sauerbrey analysis[6−8] of the frequency data overestimated the nanoparticle coverage by about a factor of 3.

RESULTS

The efficacy of cationic polystyrene nanoparticle flotation collectors was evaluated by simple beaker-scale flotation experiments in which glass beads served as model mineral particles. Figure 1 shows results from five flotation runs for 66 μm unwashed glass beads. This series of experiments employed a 5 min conditioning time, in which the glass bead and nanoparticle mixture was mixed facilitating nanoparticle deposition onto the beads before commencing the gas flow. Herein, we express the dosage of nanoparticles as the theoretical coverage, λ_T, defined as the total projected area of the nanoparticles ($n_o\pi r^2$ where r is nanoparticle radius and n_o is the nanoparticle number concentration) divided by the surface area of the glass beads. For the results in Figure 1, λ_T = 150% meaning there was enough nanoparticles to saturate the glass beads. Note, we will show below that the maximum actual

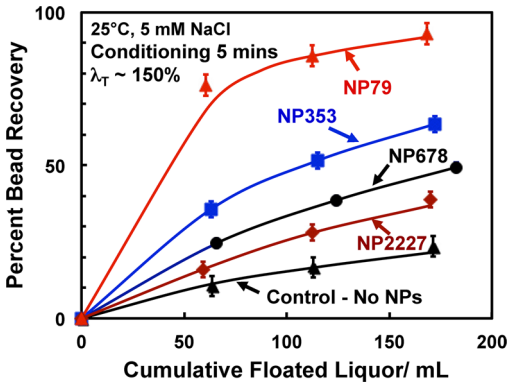

Figure 1. Glass bead (66 μm unwashed) flotation runs comparing 4 sizes of cationic polystyrene nanoparticle flotation collectors. λ_T ∼ 150% is the total nanoparticle dosage, expressed as the total projected area of deposited particles divided by the total surface area of the glass beads.

coverage we obtained for the random deposition of positively charged latex particles onto negative silica or glass was typically $\lambda_m < 40\%$.

The flotation experiments involve bubbling nitrogen through the suspension until about 60 g of aqueous foam was collected. The flotation beaker was replenished with more buffer and frother, and the gas flow resumed. The procedure was repeated resulting in three samples of collected foam phase. The control curve in Figure 1 shows the cumulative percentage of recovered glass beads as a function of the volume of liquor collected in the foam phase. The three cycles of flotation in the control curve removed 24% of the beads by a mechanism called hydrolytic entrainment, which simply represents the concentration of suspended glass beads in the liquid phase carried over with the foam.

The remaining curves were measured in the presence of nanoparticles. The most effective nanoparticle collector was NP79 (diameter 79 nm; see Table 1) giving nearly 80% recovery in the first cycle and over 90% with three cycles of flotation. The obvious conclusion from Figure 1 is that smaller nanoparticles were more effective. Nanoparticle hydrophobicity was characterized by casting smooth polymer films from organic solutions of the nanoparticle and measuring the water contact angle on the films. The contact angle results for the nanoparticles are summarized in the last column in Table 1. By this criteria, NP353 is actually more hydrophobic than NP79 and yet NP79 appears to be more effective.

The smaller nanoparticles in Table 1 were evaluated with three types of glass beads, and the flotation recovery after the first cycle is summarized in Figure 2. Again, the smaller

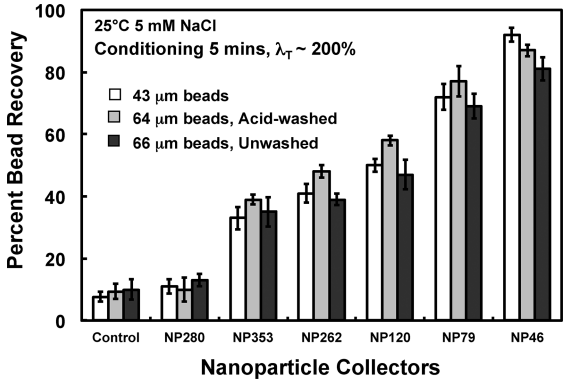

Figure 2. Comparison of cationic nanoparticles as flotation collectors for glass beads. Recovery values were based on the first dish collected, and the error bars were estimated from the experimental mass balance.

nanoparticles are more effective, and the three types of beads show the same trends. NP280 performed badly because it was a negatively charged latex meaning electrostatic forces opposed deposition on the beads instead of promoting it. The electrophoretic mobility values in Table 1 give a comparative measure of nanoparticle surface charge densities.

In an effort to gain insight into the dynamics of nanoparticle deposition onto the glass beads, particle deposition kinetics onto silica surfaces were monitored with quartz crystal microbalance (QCM-D) experiments. Figure 3A shows QCM-D frequency change as function of time for three nanoparticle sizes. The nanoparticle concentrations were 178 mg/L, and the time axes were shifted to separate the curves. At first glance, the smaller particles are depositing more quickly and the largest particles are giving the largest frequency changes at long times. The corresponding dissipation curves are shown in Figure 3B; the largest particles gave the greatest dissipation values. The dissipation curves for all three nanoparticle types showed a maximum value as the surfaces approached saturation. This is frequently observed and is explained by a stiffening of adsorbed particle layer as it approaches saturation.[9,10] The simplest model for interpreting frequency changes is the Sauerbrey equation.[6−8] Eq 1 shows a modified version of Sauerbrey equation where Γ is the deposited mass of dry nanoparticles per unit surface (mg/m^2), n is the overtone number used in the measurement, C is mass sensitivity constant for the crystal at 5 MHz ($C = 0.177$ mg·Hz^{1-}·m^{-2}), and α is an empirical correction term accounting for the mass of immobilized water. Herein, the third overtone data (i.e., $n = 3$) are presented.[11]

$$\Gamma = -\frac{C\cdot\Delta f}{n}\alpha \tag{1}$$

The Sauerbrey analysis is valid for thin, uniform, and stiff adsorbed layers. The analysis is further complicated by the fact that the Sauerbrey mass includes both nanoparticles and water immobilized around the particles. If we consider the NP120 data at long times, Δf is −500 Hz, and the corresponding Sauerbrey mass coverage is 88.5 mg/m^2. A hexagonal close packed array of 120 nm diameter polystyrene spheres has a mass coverage of 76 mg/m^2. A SEM image of the QCM-D sensor surface, at the end of the experiment, is shown in Figure 3 and image analysis showed a surface area coverage (area of particles/total area) of $\lambda_m = 36\%$ which corresponds to a mass coverage of $\Gamma_m = 30$ mg/m^2 . Therefore, the Sauerbrey mass includes significant immobilized water. To account for the immobilized water, we introduced the imperical correction term, α, into the Sauerbrey equation, which was the fraction of Sauerbrey mass gain attributable to the nanoparticles. The α values were obtained by substituting the experimental mass coverages (Γ_m), measured by image analysis, with the experimental $\Delta f_m/n$ values into eq 1. These corrected Sauerbrey mass coverages are plotted as solid lines in Figure 3D as functions of deposition time where the corresponding α values for NP46, NP120, and NP262 are 1/3, 1/3, and 1/2.5, respectively. The solid line plots in Figure 3D were based on the assumption that α in eq 1 was independent of the coverage of deposited particles. Models predicting the quantity of trapped water in layers of adsorbed particles suggest this assumption is weak at low coverages.[10]

For ideal systems, it is also possible to simulate the deposition curves from mass transport models. We used the following expression given by Petosa et al. to estimate the theoretical deposition rates in parallel plate channels.[12]

$$\text{rate} = 0.538\frac{D_f n_0}{\frac{D}{2}}\left(\frac{Peh_c}{x}\right)^{1/3} \tag{2}$$

where $Pe = (3v_{av}(D/2)^3)/(2D_f(h_c/2)^2)$ is the relevant Peclet number; $h_c = 0.5$ mm is the channel height; $x = 6$ mm is the distance from the inlet to the center of the cell; n_o is the number concentration of particles; D is the nanoparticle diameter; $v_{av} = 1.67$ μ L/s the volumetric flow rate; and $D_f = (kT)/(3\pi\eta D)$ is the diffusion coefficient at infinite dilution.

The initial deposition rate expression (eq 2) was used to calculate the mass of deposited nanoparticles as a function of time where m_{np} is the average mass of individual particles and

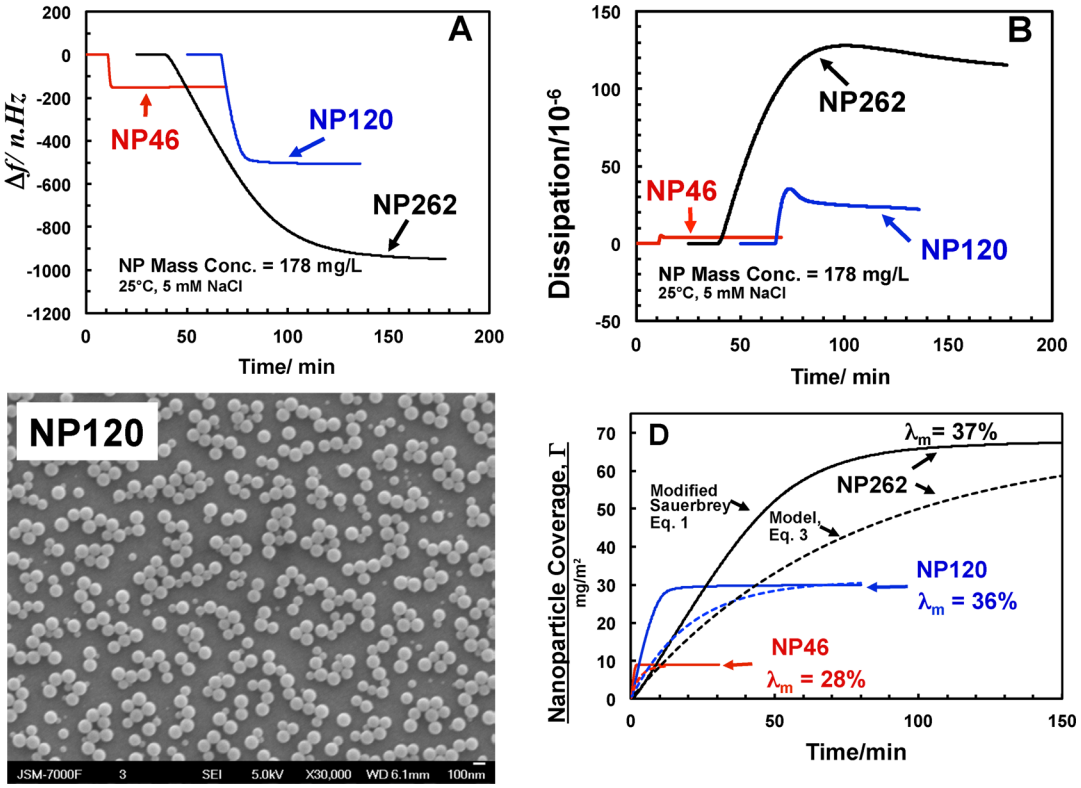

Figure 3. Nanoparticle deposition kinetics onto silica QCM-D sensor surfaces. The time axis for NP262 and NP120 were displaced for clarity. C is an SEM image of the QCM-D sensor surface after adsorption of 178 mg/L NP120. D compares the mass transport model (dashed lines calculated by eq 3) with the modified Sauerbrey (eq 1) fit to the experiment frequency data and λ_m values from SEM.

Γ_{max} is the maximum mass of particles. Γ_{max} was estimated independently from the SEM images of the sensor at the end of the experiments. Equation 3 assumes that there is no desorption of particles and there is no depletion of the particles in solution phase.

$$\frac{d\Gamma}{dt} = \text{rate} \cdot m_{np}\left(1 - \frac{\Gamma}{\Gamma_{max}}\right) \quad (3)$$

Figure 3D compares the deposition kinetics from the mass transport model with the results from the modified Sauerbrey analysis (eq 1). There are many assumptions behind the mass transport modeling and with the modified Sauerbrey analysis suggesting the quantitative analysis cannot be pushed too far. Nevertheless, both sets of curves emphasize that smaller particles deposit more quickly because the number concentration of smaller particles is greater and the deposition rate constant (eq 2) is greater for smaller particles. The maximum coverage of nanoparticles on the QCM-D silica surface ranged from 28 to 37% and was not systematically dependent upon particle size.

The nanoparticle dose is an important parameter because it is proportional to the collector cost in commercial operations. Figure 4 compares flotation results from four concentrations (expressed as λ_T) of NP79. The higher the nanoparticle dose, the higher is the cumulative bead recovery. This series of experiments was performed at a constant and rather short conditioning time of 5 min. One approach to achieving higher flotation performance with a given dose is to give a longer conditioning time to promote a greater coverage of adsorbed nanoparticles before flotation starts. Figure 5 illustrates the role of conditioning time for NP353. The greatest improvements

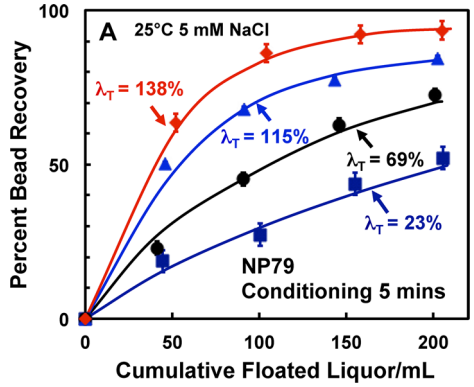

Figure 4. Flotation recovery of 2 g of 66 μm unwashed glass beads by adding various dosages of 18.6 g/L NP79 (0.05 mL, 0.15 mL, 0.25 mL, and 0.30 mL, equivalent to 0.23, 0.69, 1.15, and 1.38 times the glass bead surface area) for 5 min conditioning in 5 mM NaCl.

corresponded to going from 5 to 30 min conditioning whereas there was little advantage going from 30 to 60 min conditioning.

In many of our flotation experiments, both nanoparticle decorated beads and free nanoparticles were present in the flotation liquor. We wished to determine if free nanoparticles in water were removed by flotation. Three types of nanoparticles were evaluated in flotation experiments without glass beads, and the results are summarized in Table 2. There was no significant enrichment of nanoparticles in the froth meaning gas bubbles did not collect the nanoparticles. These results are consistent with published studies of small particle flotation.[13]

dx.doi.org/10.1021/am301215h | ACS Appl. Mater. Interfaces 2012, 4, 4882−4890

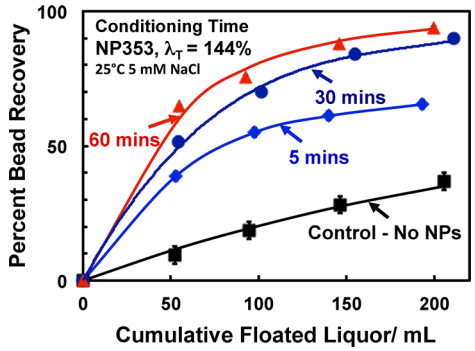

Figure 5. Influence of the time allowed for nanoparticles to deposit onto 64 μm acid-washed glass beads on the recovery of glass beads. The dosage of NP353 nanoparticles was equivalent to 1.44 times the glass bead surface area. The error bars estimated from replicated experiments were smaller than the points for all but the control experiment.

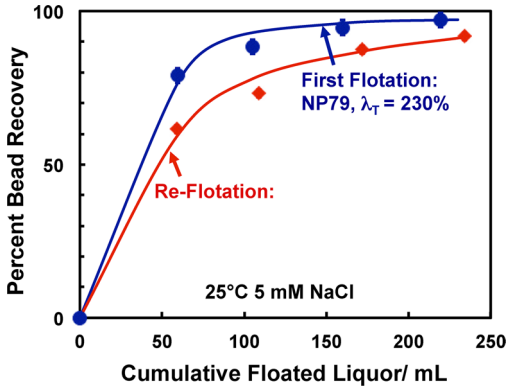

Figure 6. Comparison of the flotation run of 2 g of 66 μm unwashed glass beads by excess addition of 0.5 mL of 18.6 g/L NP79 (λ_T = 230%) with the follow-up reflotation of the 1.95 g of dried recovered beads from the initial flotation.

The interpretation of the flotation results so far presented is complicated by the coupling of the kinetics of nanoparticle adsorption with the flotation kinetics. Nanoparticles are much larger than conventional molecular collectors causing the nanoparticle adsorption time scales to be similar to the flotation time scales. In an effort to gain more fundamental understanding, we have treated glass beads with nanoparticles, followed by removing excess unadsorbed nanoparticle after which we performed flotation experiments. Flotation results for NP46 and NP120 are shown as a function of the actual coverage of nanoparticles in Figure 7. By comparing nanoparticle size effects at a given coverage, we are factoring out the influence of nanoparticle deposition kinetics. NP120 and NP79 are significantly less effective than NP46. The contact angle of NP120 was 8 degrees less than NP46, which seems too small to explain the difference. Therefore, we propose that these results show that smaller nanoparticles are better collectors for smooth, clean glass beads.

We have many electron micrographs of glass beads coated with our nanoparticles, and we have seen little evidence that the adsorbed nanoparticles are being moved or even removed by capillary forces. To illustrate the strong adhesion, we performed a flotation, collected the floated beads, rinsed them, and performed a second flotation without an additional collector. The two flotation runs are shown in Figure 6, and there was little degradation in flotation performance with the recovered, washed beads. We propose that this is evidence for strong adhesion with the adsorbed smaller nanoparticles.

DISCUSSION

Understanding the role of nanoparticle size in their application as flotation collectors is an important aspect of the development of design rules for nanoparticle flotation collectors. In every experiment comparing glass bead flotation recovery with cationic polystyrene nanoparticle flotation collectors, small particles were more effective than larger ones. Indeed, the results in Figure 2 suggest a monotonic, inverse relationship between nanoparticle size and flotation recovery. Before discussing possible explanations, the current understanding of flotation fundamentals is briefly summarized to give context for our discussion.

At a superficial level, the sequence of events are: nanoparticle deposition onto glass beads; glass bead attachment to air bubbles; air bubbles rise into the foam phase that is removed. A recent text edited by Fuerstenau, Jameson, and Yoon[3] gives a good summary of the current understanding of flotation mechanisms. A typical approach to flotation modeling is to divide flotation into a sequence of steps and to develop a probability expression for each step. Nanoparticle flotation collectors are likely to influence two important steps in the sequence of flotation mechanisms: the attachment of the mineral particle to the air bubble surface after collision and the unwanted detachment of the mineral particles from the bubbles. Nguyen et al. argues that the attachment step involves three processes: (1) thinning of the intervening liquid film between the mineral particle and the bubble; (2) rupture of the film to give a three phase contact "nucleus"; and (3) expansion of the three phase contact line (TPCL) from the nucleus to form a stable wetting perimeter.[14]

Nanoparticle Diameter Influence on Deposition Kinetics. A necessary condition for flotation is the deposition of the hydrophobic nanoparticles onto the hydrophilic glass beads. The colloid literature teaches us that small particles diffuse more quickly giving a faster deposition rate constant.[15] Our quartz crystal microbalance deposition studies onto a silica

Table 2. Selective Control Flotation Experiments of Nanoparticles Only in 125 mL, 5 mM NaCl in the Presence of 10 mg/L Frother[a]

nanoparticle	starting conc., mg/L	floated liquor conc., mg/L	floated liquor volume, mL	nanoparticle recovery, wt %	enrichment factor
NP262	200	207 ± 5.2	63 ± 3.1	54 ± 2.6	1.1
NP120	220	261 ± 4.3	65 ± 1.5	61 ± 1.7	1.2
NP280	320	308 ± 6.3	56 ± 4.2	44 ± 3.5	0.98
–	–	–	57 ± 1.8	–	–

[a]The standard errors were calculated from three replicated flotation runs. Enrichment factor represents the percent recovered nanoparticles divided by the percent floated liquid.

surface in Figure 3 illustrates these behaviors. The initial deposition rate of the smallest particles was 150 times greater than the largest nanoparticles whereas at long deposition times the maximum coverage of the three nanoparticles varied only from 28 to 37%. The maximum packing of randomly deposited hard spheres is about 55%; lower values arise from electrostatic repulsion between nanoparticles.[16]

For the flotation experiments whose results are summarized in Figures 1, 4, and 5, the nanoparticles were added to the glass beads and mixed for conditioning times followed by flotation. The resulting flotation curves reflect the coupling of the nanoparticle deposition kinetics with the flotation kinetics. Increasing nanoparticle concentration or conditioning time gave higher coverages of adsorbed nanoparticles, in turn, giving higher bead recoveries. These behaviors underscore the requirement for long conditioning times to give the dilute nanoparticle suspensions time to deposit onto mineral surfaces.

Flotation Recovery versus Nanoparticle Diameter at Constant Coverage. Figure 7 shows that, when comparing to nanoparticles at the same coverage, the smaller particles are more effective. Note the NP46 and NP120 curves were obtained in experiments in which the nanoparticles were deposited onto the beads and the nondeposited nanoparticles were decanted away before flotation. This comparison eliminates the influence of nanoparticle transport and deposition onto the bead surfaces. Therefore, it appears that smaller particles are intrinsically superior when compared at the same coverage. The water contact angles on smooth polymer films cast from dissolved nanoparticles (last column in Table 1) were approximately the same. Although the smallest particles were slightly more hydrophobic, we do not believe the differences were great enough to explain the large differences in flotation efficiency. The following paragraphs discuss the potential role of nanoparticle diameter in the various steps in flotation; the relevant relationships are summarized Table 3.

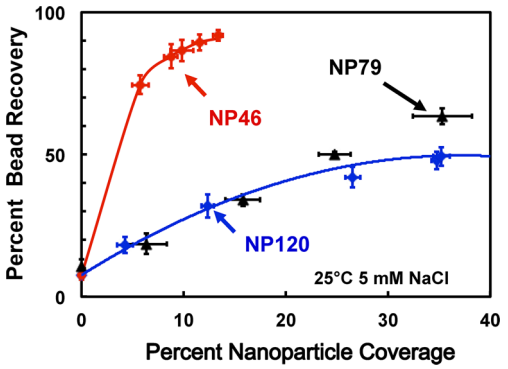

Figure 7. Flotation recovery as functions of coverage for three nanoparticles. NP46 and NP120 results were with 43 μm beads, and the unadsorbed nanoparticles were decanted from the beads before flotation. NP79 results were for 66 μm unwashed glass beads, and the unadsorbed latex was not removed before flotation.

The mineral−air−water contact angle is an important parameter in a number of the theories. Previously, we have shown that the contact angle of water on glass decorated with our nanoparticles approximately obeys the Cassie−Baxter relation (Row 1 in Table 3). There are only three parameters dictating the resulting contact angle in the Cassie−Baxter model: the coverage, λ, and the intrinsic contact angle of the nanoparticle surface, θ_{np}, determine the contact angle, and the water contact angle on the nanoparticle-free mineral, θ_{sil}.[2] At a given coverage, λ, the Cassie−Baxter predicts that the contact angle is independent of nanoparticle diameter; see Row 1 in Table 3.

The first step in flotation is the initial attachment of a mineral particle to a bubble to give what Ralston describes as a "contact nucleus". Many published theoretical analyses of attachment reveal that attachment probability is dominated by hydrodynamics.[3] Smaller mineral particles have low attachment efficiency as they follow the streamlines around bubbles, whereas larger minerals have sufficient momentum to approach the air/water interface. Most of our results correspond to comparisons where the glass bead particle size and the hydrodynamic conditions were constant. We presume that the nanoparticles only potentially influence the final stages of the contact nucleus formation during the drainage of the thin aqueous film separating the glass beads from the air bubbles. For attachment, the characteristic film drainage time must be small, consistent with the mineral/bubble encounter time. The

Table 3. Relevant Models Giving Insight into the Role of Nanoparticle Diameter in Flotation[a]

row #	effect	model	reference
1	contact angle: no particle size dependence	$\cos(\theta) = \lambda\cos(\theta_{np}) + (1 - \lambda)\cos(\theta_{sil})$	Cassie−Baxter equation for a mixed surface composition.[21,22]
2	contact nucleus formation; see Figure 8: probability of attachment increases with D	$t_a \approx \frac{1}{D^2}$ $p_c \approx \frac{1}{t_a} \approx D^2$	Proposed herein in analogy with defoamer particle mechanisms.[17,18]
3	TPCL expansion over smooth, uniform surfaces: does not account for nanoparticles	$D_{min} = 2\left[\frac{3r_c^2\gamma(1 - \cos(\theta))}{\Delta\rho V^2}\right]^{1/3}$	Drelich's model gives the minimum diameter of a mineral particle, D_{min}, that can be floated.[23]
4	TPCL expansion over hydrophilic surfaces decorated with more hydrophobic nanoparticles. We postulate inverse dependence on D.	$d_{ss} = \frac{D}{2}\left(\sqrt{\frac{\pi}{\lambda}} - 1\right)$ $p_e \approx \frac{1}{d_{ss}} \approx \frac{1}{D}$	d_{ss} relation was described previously.[1] p_e relation proposed here.
5	pull-off force: independent of D	$F = 2\pi R_m\gamma\sin^2\left(\frac{\theta}{2}\right)$	Scheludko's model for the force, F, required to dislodge a mineral particle from a bubble.[5,20]

[a]See symbol list for symbols not defined in the table.

drainage of thin water films (lamellae) has been much discussed in the foam stability and the defoamer literature.[17−19] For example, the presence of hydrophobic nanoparticles on an oil drop in water facilitates the attachment of the oil to air bubbles because the water film only needs to drain sufficiently for the hydrophobic nanoparticle to contact the air.[19] We propose the same occurs with the attachment of mineral particles coated with hydrophobic nanoparticles; see illustration in Figure 8.

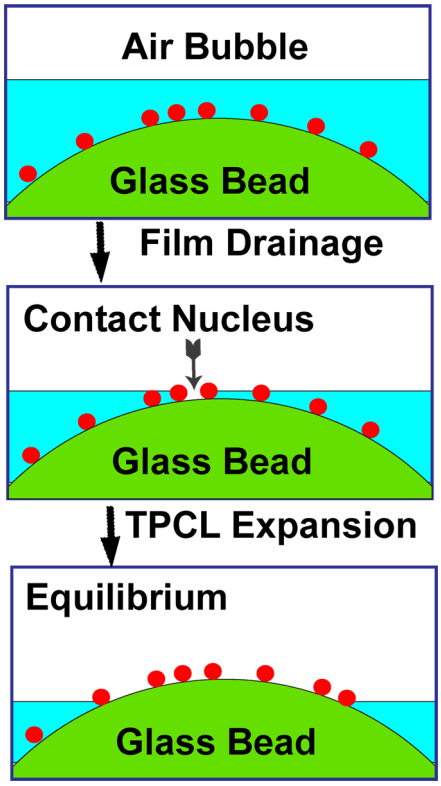

Figure 8. Nanoparticles inducing contact nucleus formation; the initial stages of particle-air bubble attachment. We propose that larger nanoparticle diameters promote contact nucleus formation wheres smaller nanoparticles promote TPCL expansion.

Lacking a detailed model, we propose that the characteristic time to form a contact nucleus, t_a, is the time required for the water film to drain to a thickness corresponding to the nanoparticle diameter. The foam lamella drainage literature predicts that drainage time scales with the inverse of the square of the film thickness (Row 2 in Table 3).[18] These assumptions lead to prediction that the probability of contact nucleus formation increases with nanoparticle diameter. Thus, contract nucleus formation does not predict our observations that small nanoparticles are more efficient.

After contact nucleus formation, the three phase contact line (TPCL) expands to an equilibrium contact patch. Row 3 in Table 3 gives Drelich and Millar's model for the minimum mineral diameter that can be floated based on TPCL expansion. This relationship was developed for smooth mineral particles and does not address the presence of discrete hydrophobic particles. With a hydrophilic surface decorated with hydrophobic nanoparticles, the segments of the TPCL must jump from one hydrophobic particle over hydrophilic patches to the next hydrophobic particle. We propose that the smaller the distance between neighboring particles, the higher is the probability that the TPCL will advance. The relationships in Row 4 in Table 3 shows that the distance between neighboring particle surfaces is proportional to nanoparticle diameter, D, and inversely related to the square root of the coverage, λ. We propose that the corresponding probability of three TPCL expansion scales with the inverse of the nearest neighbor distance and thus the inverse of nanoparticle diameter. The specific relationship for d_{ss} (Row 4 in Table 3) was derived for a square array. The random distribution of nanoparticles more relevant to our experiments should give a similar scaling with nanoparticle diameter.

Finally, the nanoparticles must generate sufficiently high capillary forces such that the mineral particles (or glass beads in our case) do not detach. Row 5 in Table 3 gives Scheludko's classical expression that predicts no nanoparticle dependence in the detachment or pull-off forces.[5,20] In our first publication in this series, we developed a related expression that accounted for the specific role of the nanoparticles; our model also predicted no influence of nanoparticle diameter on pull-off forces.[1]

In summary, only the relationship in Row 4 of Table 3 suggests that smaller nanoparticles will be more effective at a constant coverage and nanoparticle hydrophobicity. Recognizing we give only a hand waving rationalization for the inverse relationship between p_e and D, we propose that the influence of nanoparticle diameter on expansion of the TPCL explains the superiority of smaller particles when considered at constant coverage (see Figure 7).

Since the experiments and the explanations herein support the hypothesis "smaller is better", an obvious question is why use nanoparticles as flotation collectors: surely, the very small and well-established molecular collectors such as alkyl xanthates are superior? We envisage two situations where nanoparticles may offer advantages. First, in those cases where the mineral surface is contaminated with nanosize slime such as serpentine fibers, the hydrophobic nanoparticles may perform better than thin patches of molecular collector that are buried under the slime. Second, in cases where the air bubbles are particularly stable and thus resistant to formation of the initial contact nucleus, nanoscale hydrophobic protuberances on the mineral surface should facilitate rupture of the aqueous film separating the air bubble and mineral particle; similar approaches are used in defoamer technology to nucleate rupture of foam lamellae.[18] Neither of these two situations were evaluated herein; however, future publications involving more practical mineral systems will demonstrate the utility of nanoparticle flotation collectors.

CONCLUSIONS

(1) Although there are no energy barriers to the deposition of cationic polystyrene nanoparticles onto anionic glass, under the conditions of our flotation experiments, a 5 to 30 min conditioning (deposition) time was required for sufficient coverages to give high flotation recoveries (yields). (2) For clean, smooth glass bead flotation, smaller hydrophobic cationic polystyrene particles are more effective. Although definitive explanations are difficult to prove, our evidence supports the following explanations: (a) Smaller nanoparticles deposit more quickly than larger ones because they diffuse more quickly to the mineral/water interface and, because at a constant mass concentration, the number concentration of nanoparticles is higher. We believe that deposition kinetics is the dominant time effect. (b) When the total dosage of nanoparticles is much lower than required to saturate the mineral surfaces, a given mass of smaller nanoparticles will cover a greater percentage of the mineral surface, giving a higher contact angle. (c) Flotation

experiments involving beads with predeposited nanoparticles also showed that smaller is better when comparing at constant coverage. We propose that, during bead−air bubble attachment, the distance that the three phase contact line must jump over hydrophilic domains decreases with particle size, facilitating attachment. (3) For nanoparticle diameters up to 79 nm, we see no evidence of nanoparticle desorption from the bead surfaces. Indeed, recovered beads can be refloated without an additional collector. (4) The hydrophobic nanoparticles are not removed by flotation in the absence of beads (mineral).

■ ASSOCIATED CONTENT

Supporting Information

Methods and recipes for nanoparticle synthesis; some nanoparticle electron micrgraphs; nanoparticle electrophoretic mobility vs pH; glass bead particle size distributions. This information is available free of charge via the Internet at http://pubs.acs.org/

■ AUTHOR INFORMATION

Corresponding Author

*E-mail: peltonrh@mcmaster.ca.

Notes

The authors declare no competing financial interest.

■ ACKNOWLEDGMENTS

We thank the Centre for Materials and Manufacturing (CMM), a division of the Ontario Centres of Excellence (OCE) in collaboration with VALE Base Metals for funding, VALE Base Metals Technology Development for funding, Zongfu Dai and Manqiu Xu from Vale for help, samples, and advice. We also acknowledge Ms. Alexis Ambeault for acquiring some electrophoretic mobility data.

■ SYMBOLS

α = the fraction of the Sauerbrey mass due to nanoparticles; eq 1
$\Delta\rho$ = the density difference between the mineral and water
Δf = the QCM-D frequency shift (Hz); eq 1
γ = the surface tension
Γ = mass coverage of nanoparticles (mg/m^2)
Γ_m = the maximum mass coverage measured at the end of an experiment (mg/m^2)
λ = the surface coverage (i.e., fraction of glass bead surface area covered by nanoparticles)
λ_T = the dosage of added nanoparticles expressed as a surface coverage
λ_m = the fraction of glass bead surface area covered by nanoparticles at the end of an experiment
η = the aqueous phase viscosity
θ = the contact angle of air bubble/bead/water three phase contact line (TPCL)
θ_{np} = the contact angle of water on nanoparticle
θ_{sil} = the contact angle of water on clean glass bead surface
C = the mass sensitivity constant for QCM-D crystal (C = 0.177 mg/m^2·Hz); eq 1
d_{ss} = the distance between surfaces of neighboring nanoparticles in a square array on a surface[1]
D = the nanoparticle diameter
D_f = the nanoparticle diffusion coefficient; eq 2
D_{min} = the minimum diameter of a mineral particle that can be floated
F = the maximum force required to pull a mineral particle off of a bubble
h_c = 0.5 mm is channel height in the QCM-D cell; eq 2
m_{np} = the mass of an individual nanoparticle
p_c = the probability contact nucleus formation between bead and bubble
p_e = the probability of the TPCL expanding from the contact nucleus to a stable dry patch on the mineral surface
P_e = the Peclet number; eq 2
n_o = the initial number concentration of nanoparticles (m^{-3}); eq 2
r_c = the critical bubble radius below which there is no bubble attachment to the mineral surface
R_m = the radius of the mineral particle (i.e., glass bead radius) that can be floated
t_a = the time for the water film between mineral and bubble to drain to the point of contact with a bubble
v_{av} = 1.67 μL/s; the volumetric flow rate in the QCM-D cell
V = the bubble assent velocity
x = 6 mm; the distance from the inlet to the center of the QCM-D cell; eq 2

■ REFERENCES

(1) Yang, S.; Pelton, R.; Raegen, A.; Montgomery, M.; Dalnoki-Veress, K. *Langmuir* **2011**, *27* (17), 10438−10446.
(2) Yang, S.; Pelton, R. *Langmuir* **2011**, *27* (18), 11409−11415.
(3) Fuerstenau, M.; Jameson, G.; Yoon, R. *Froth Flotation: A Century of Innovation*; Society for Mining, Metallurgy, and Exploration: Littleton, CO, 2007.
(4) Trahar, W. J.; Warren, L. J. *Int. J. Miner. Process.* **1976**, *3* (2), 103−131.
(5) Scheludko, A.; Toshev, B. V.; Bojadjiev, D. T. *J. Chem. Soc., Faraday Trans. 1* **1976**, *72*, 2815−2828.
(6) Sauerbrey, G. *Z. Phys.* **1959**, *155*, 206−222.
(7) Höök, F.; Rodahl, M.; Brzezinski, P.; Kasemo, B. *Langmuir* **1998**, *14* (4), 729−734.
(8) Edvardsson, M.; Rodahl, M.; Kasemo, B.; Höök, F. *Anal. Chem.* **2005**, *77* (15), 4918−4926.
(9) Johannsmann, D.; Reviakine, I.; Richter, R. P. *Anal. Chem.* **2009**, *81* (19), 8167−8176.
(10) Bingen, P.; Wang, G.; Steinmetz, N. F.; Rodahl, M.; Richter, R. P. *Anal. Chem.* **2008**, *80* (23), 8880−8890.
(11) Fatisson, J.; Domingos, R. F.; Wilkinson, K. J.; Tufenkji, N. *Langmuir* **2009**, *25* (11), 6062−6069.
(12) Petosa, A. R.; Jaisi, D. P.; Quevedo, I. R.; Elimelech, M.; Tufenkji, N. *Environ. Sci. Technol.* **2010**, *44* (17), 6532−6549.
(13) Nguyen, A. V.; George, P.; Jameson, G. J. *Chem. Eng. Sci.* **2006**, *61* (8), 2494−2509.
(14) Nguyen, A. V.; Schulze, H. J.; Ralston, J. *Int. J. Miner. Process.* **1997**, *51* (1−4), 183−195.
(15) Van de Ven, T. *Colloidal Hydrodynamics*; Academic Press: London, 1989; p 582.
(16) Adamczyk, Z.; Zembala, M.; Siwek, B.; Warszynski, P. *J. Colloid Interface Sci.* **1990**, *140* (1), 123−137.
(17) Frye, G. C.; Berg, J. C. *J. Colloid Interface Sci.* **1989**, *127* (1), 222−238.
(18) Garrett, P. *Defoaming: Theory and Industrial Applications*; CRC Press: Boca Raton, FL, 1993.
(19) Wang, G.; Pelton, R.; Hrymak, A.; Shawafaty, N.; Heng, Y. M. *Langmuir* **1999**, *15* (6), 2202−2208.
(20) Fielden, M. L.; Hayes, R. A.; Ralston, J. *Langmuir* **1996**, *12* (15), 3721−3727.
(21) Cassie, A. B. D.; Baxter, S. *Trans. Faraday Soc.* **1944**, *40*, 546−551.
(22) De Gennes, P. G.; Brochard-Wyart, F.; Quéré, D. *Capillarity and Wetting Phenomena: Drops, Bubbles, Pearls, Waves*; Springer Verlag: New York, 2004.

(23) Drelich, J.; Miller, J. D. *Colloids Surf.* **1992**, *69* (1), 35−43.